A RELATIONAL INTERVENTION APPROACH FOR UNSUPERVISED DYNAMICS GENERALIZATION IN MODEL-BASED REINFORCEMENT LEARNING

Anonymous authors
Paper under double-blind review

ABSTRACT

The generalization of model-based reinforcement learning (MBRL) methods to environments with unseen transition dynamics is an important yet challenging problem. Existing methods try to extract environment-specified information Z from past transition segments to make the dynamics prediction model generalizable to different dynamics. However, because environments are not labelled, the extracted information inevitably contains redundant information unrelated to the dynamics in transition segments and thus fails to maintain a crucial property of Z: Z should be similar in the same environment and dissimilar in different ones. As a result, the learned dynamics prediction function will deviate from the true one, which undermines the generalization ability. To tackle this problem, we introduce an interventional prediction module to estimate the probability of two estimated $\hat{z}_i, \hat{z}_j$ belonging to the same environment. Furthermore, by utilizing the Z's invariance within a single environment, a relational head is proposed to enforce the similarity between $\hat{Z}$ from the same environment. As a result, the redundant information will be reduced in $\hat{Z}$. We empirically show that $\hat{Z}$ estimated by our method enjoy less redundant information than previous methods, and such $\hat{Z}$ can significantly reduce dynamics prediction errors and improve the performance of model-based RL methods on zero-shot new environments with unseen dynamics.

1 INTRODUCTION

Reinforcement learning (RL) has shown great success in solving sequential decision-making problems, such as board games (Silver et al., 2016; 2017; Schrittwieser et al., 2020), computer games (*e.g.* Atari, StarCraft II) (Mnih et al., 2013; Silver et al., 2018; Vinyals et al., 2019), and robotics (Levine & Abbeel, 2014; Bousmalis et al., 2018). However, solving real-world problems with RL is still a challenging problem because the sample efficiency of RL is low while the data in many applications is limited or expensive to obtain (Gottesman et al., 2018; Lu et al., 2018; 2020; Kiran et al., 2020). Therefore, model-based reinforcement learning (MBRL) (Janner et al., 2019; Kaiser et al., 2019; Schrittwieser et al., 2020; Zhang et al., 2019b; van Hasselt et al., 2019; Hafner et al., 2019b;a; Lenz et al., 2015), which explicitly builds a predictive model to generate samples for learning RL policy, has been widely applied to a variety of limited data sequential decision-making problems.

However, the performance of MBRL methods highly relies on the prediction accuracy of the learned environmental model (Janner et al., 2019). Therefore, a slight change of environmental dynamics may cause a significant performance decline of MBRL methods (Lee et al., 2020; Nagabandi et al., 2018a; Seo et al., 2020). The vulnerability of MBRL to the change of environmental dynamics makes them unreliable in real world applications. Taking the robotic control as an example (Nagabandi et al., 2018a; Yang et al., 2020; Rakelly et al., 2019; Gu et al., 2017; Bousmalis et al., 2018; Raileanu et al., 2020; Yang et al., 2019), dynamics change caused by parts damages could easily lead to the failure of MBRL algorithms. This problem is called the *dynamics generalization* problem in MBRL, where the training environments and test environments share the same state $\mathcal{S}$ and action space $\mathcal{A}$ but the transition dynamics between states $p(s_{t+1}|s_t, a_t)$ varies across different environments. Following previous works (Petersen et al., 2018; Gottesman et al., 2018), we focus on the **unsupervised dynamics generalization** setting, *i.e.* the id or label information of dynamics function in training MDPs is not available. This setting appears in a wide range of applications where the information of

dynamics function is difficult to obtain. For example, in healthcare, patients may respond differently to the same treatment, *i.e.*, $p(s_{t+1}|s_t, a_t)$ varies across patients. However, it is difficult to label which patients share similar dynamics.

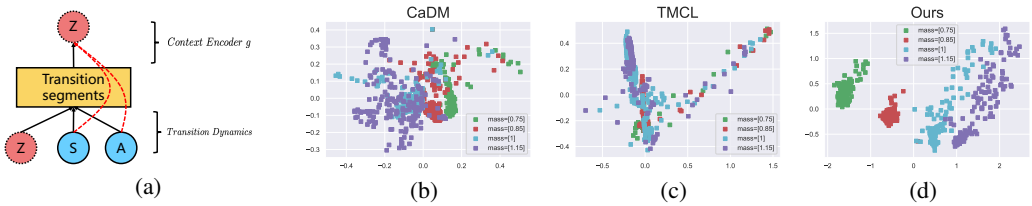

(a) (b) (c) (d)

Figure 1: (a) The illustration of why historical states and actions are encoded in environment-specified factor Z, (b)(c)(d) The PCA visulization of estimated context (environmental-specific) vectors in **Pendulum** task, where the dots with different colors denote that the context vector (after PCA) estimated from different environments. More visualization results are given at Appendix A.13.

To build a generalized dynamics prediction function that can generalize to different transition dynamics, the shift of the transition dynamics can be modelled as the change of unobserved factors across different environments, *i.e.* there are hidden environment-specified factors $Z \in \mathcal{Z}$ which can affect the environmental dynamics. This is analogous to the human intuition to understand the change of dynamics, *e.g.* patients may show different responses to identical treatments because the differences of their gene sequences can affect how well they absorb drugs (Wilke et al., 2007). It is natural to assume that Z is the same in a single environment but varies across different environments. As such, these unobserved environment-specified factors do not violate the nature of MDP in a single environment, but their changes can affect the dynamics functions across environments. Therefore, the dynamics function $f : \mathcal{S} \times \mathcal{A} \to \mathcal{S}$ can naturally be augmented by incorporating Z to be $f : \mathcal{S} \times \mathcal{A} \times \mathcal{Z} \to \mathcal{S}$ (Rakelly et al., 2019; Zhou et al., 2019; Lee et al., 2020; Seo et al., 2020).

Learning the augmented dynamics function is difficult because the environment-specified factor Z is unobservable. Previous methods (Rakelly et al., 2019; Zhou et al., 2019; Lee et al., 2020) try to extract information from historical transition segments and use it as a surrogate for Z (Figure 1a) . However, in the unsupervised dynamics generalization setting, the extracted information from historical transition segments inevitably contains redundant information unrelated to the dynamics in transition segments. The redundant information would cause the surrogate for Z to lose a crucial property that characterizes Z: Z should be similar in the same environment and dissimilar in different environments. As shown in Figure 1b, the learned environment-specified information of a state-of-the-art method CaDM (Lee et al., 2020) does not form clear clusters for different environments. Because the learned $\hat{Z}$ fails to represent environmental information, the learned dynamics prediction function will deviate from the true one, which undermines the generalization ability. To alleviate this problem, TMCL (Seo et al., 2020) directly clusters the environments by introducing multiple prediction heads, *i.e.* multiple prediction functions. However, TMCL needs to choose the proper prediction head for each new environment, making it hard to be deployed into the scenario with consistently changing environments, *e.g.* robots walk in the terrain which is constantly changing. To avoid adaptation at the deployment time, we thus need to learn a single generalized prediction function $\hat{f}$. To ensure that $\hat{f}$ can learn modals of transition dynamics in different environments, we need to cluster Z according to their belonging environment.

In this paper, we provide an explicit and interpretable description to learn Z as a vector $\hat{Z}$ (*i.e.* the estimation of Z) from the history transition segments. To cluster $\hat{Z}$ from the same environment, we introduce a relational head module as a learnable function to enforce the similarity between $\hat{Z}$s learned from the same environments. However, because environment label is not available, we can only cluster the $\hat{Z}$s from the same trajectory, so we then propose an interventional prediction module to identify the probability of a pair of $\hat{z}_i, \hat{z}_j$ belonging to the same environment through estimating $\hat{Z}$'s direct causal effect on next states prediction by do-calculus (Pearl, 2000). Because Z from the same environment surely have the same causal effect, we can directly maximize the similarity of $\hat{Z}$s with the similar causal effect using the relational head, and thus can cluster $\hat{Z}$ according to the estimated environmental similarity and alleviate the redundant information that varies in an environment, *e.g.* historical states and actions. In the experiments, we evaluate our method on a range of tasks in OpenAI gym (Brockman et al., 2016) and Mujoco (Todorov et al., 2012), and empirically show that $\hat{Z}$ estimated by our method enjoy less redundant information than baselines, and the experimental

results show that our method significantly reduces the model prediction errors and outperforms the state-of-art model-based RL methods **without any adaptation step** on a new environment, and even achieve comparable results with the method directly cluster $\hat{Z}$ with the true environment label.

2 Related Work

Dynamics Generalization in MBRL Several meta-learning-based MBRL methods are proposed Nagabandi et al. (2018a;b); Sæmundsson et al. (2018) to adapt the MBRL into environments with unseen dynamics by updating model parameters via a small number of gradient updates Finn et al. (2017) or updating hidden representations of a recurrent model Doshi-Velez & Konidaris (2016), and then Wang & van Hoof (2021) proposes the graph structured model to model the dynamics accurately to improve dynamics forecasting. Ball et al. (2021) focus on the offline setting and proposes an augmented model method to achieve zero-shot generalization. Lee et al. (2020); Seo et al. (2020) try to learn a generalized dynamics model by incorporating context information or clustering dynamics implicitly using multi-choice learning, aiming to adapt any dynamics without training. However, how to explicitly learn the meaningful dynamics change information remains a big challenge.

Relational Learning Reasoning relations between different entities is a way to build knowledge of this world for intelligent agents Kemp & Tenenbaum (2008). In the past decades, relational paradigm have been applied to a wide range of deep learning-based application, *e.g.*, reinforcement learning Zambaldi et al. (2018), question answer Santoro et al. (2017); Raposo et al. (2017), graph neural network Battaglia et al. (2018), sequential streams Santoro et al. (2018), few-shot learning Sung et al. (2018), object detection Hu et al. (2018) and self-supervised learning Patacchiola & Storkey (2020). Different from previous methods that perform binary relational reasoning on entities, our method can also perform multiplies relations between entities through the learned similarity of entities, and thus can learn more compact and meaningful entity representation.

Causality in Reinforcement Learning Many works focus on the intersection area of reinforcement learning and causal inference. For example, some works aims to alleviate the causal confusion problem in the imitation learning (de Haan et al., 2019; Zhang et al., 2020c; Kumor et al., 2021), batch learning (Bannon et al., 2020), and partial observability settings (Forney et al., 2017; Kallus & Zhou, 2018; Zhang et al., 2019a; Lu et al., 2018) in the online environment (Lyle et al., 2021; Zhang & Bareinboim, 2018), (Wang et al., 2020) also try to apply causal inference in the offline setting, where the observational data is always confounded. Lee & Bareinboim (2018); Bareinboim et al. (2015); Lattimore et al. (2016); Mozifian et al. (2020); Volodin et al. (2020) also explore how to design an optimal intervention policy in bandits or RL settings. In addition, (Zhang et al., 2020a;b) improve the generalization ability of state abstraction. Different from these methods, we focus on the setting of unsupervised dynamics generalization, and measure the direct causal effect (Pearl, 2013) between $\hat{Z}$ and the next state to estimate the probability of them belonging to the same environment.

3 Methods

In the section, we first introduce the formulation of the dynamic generalization problem. Then we present the details on how relational intervention approach learns the environment-specified factors.

3.1 Problem Setup

The standard reinforcement learning task can be formalized as a Markov decision process (MDP) $\mathcal{M} = (\mathcal{S}, \mathcal{A}, r, p, \gamma, \rho_0)$ over discrete time (Puterman, 2014; Sutton & Barto, 2018), where $\mathcal{S}$, $\mathcal{A}$, $\gamma \in (0, 1]$, ρ_0 are state space, action space, the reward discount factor, and the initial state distribution, respectively. The reward function $r : \mathcal{S} \times \mathcal{A} \to \mathbb{R}$ specifies the reward at each timestep t given s_t and a_t, and transition dynamics $p(s_{t+1}|s_t, a_t)$ gives the next state distribution conditioned on the current state s_t and action a_t. The goal of RL is to learn a policy $\pi(\cdot|s)$ mapping from state $s \in \mathcal{S}$ over the action distribution to maximize the cumulative expected return over timesteps $\mathbb{E}_{s_t \in \mathcal{S}, a_t \in \mathcal{A}}[\sum_{t=0}^{\infty} \gamma^t \, r(s_t, a_t)]$. In model-based RL, a model f is used to approximate the transition dynamics p, and then f can provide training data to train policy π or predict the future sequences for planning. Benefiting from data provided by learned dynamics model f, model-based RL has higher data efficiency and better planing ability compared with model-free RL.

Here we consider the unsupervised *dynamics generalization* problem in model-based RL, where we are given K training MDPs $\{\mathcal{M}_i^{tr}\}_{i=1}^K$ and L test MDPs $\{\mathcal{M}_j^{te}\}_{j=1}^L$ that have the same state and action space but disjoint dynamics functions, and we randomly sample several MDPs from training MDPs in each training iteration. We assume that all these MDPs have a finite number of dynamics functions, meaning that the MDPs can be categorized into a finite number of environments and the MDPs in each environment share the same dynamics function but the environment id of MDPs is unavailable in the training process. In the context of model-based RL, how to learn a generalized dynamics model f is the key challenge to solve unsupervised *dynamics generalization* problem.

3.2 Overview

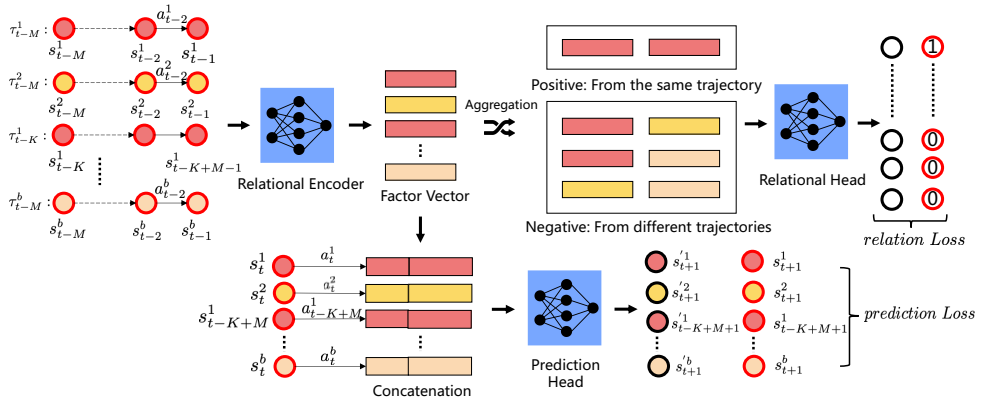

Figure 2: An overview of our Relational Intervention approach, where Relational Encoder, Prediction Head and Relational Head are three learnable functions, and the circles denote states (Ground-Truths are with red boundary, and estimated states are with black boundary), and the rectangles denote the estimated vectors. Specifically, $prediction\ Loss$ enables the estimated environmental-specified factor can help the Prediction head to predict the next states, and the $relation\ Loss$ aims to enforce the similarity between factors estimated from the same trajectory or similar trajectories.

As analyzed in Section 1, we can incorporate the environment-specified factors $Z \in \mathcal{Z}$ into the dynamics prediction process to generalize the dynamic functions on different environments, *i.e.* extending the dynamics function from $f : \mathcal{S} \times \mathcal{A} \rightarrow \mathcal{S}$ to $f : \mathcal{S} \times \mathcal{A} \times \mathcal{Z} \rightarrow \mathcal{S}$. Because Z is the same within an environment, we expect estimated $\hat{Z}$s from the same environment are similar while those from different environments are dissimilar. Therefore, f models the commonalities of the transition dynamics in different environments and Z models the differences. In the supervised dynamics generalization setting, where the environment id is given, one can easily learn Z by using metric losses, *e.g.*, CPC (Oord et al., 2018) and relation loss (Patacchiola & Storkey, 2020) to enforce that the estimated $\hat{Z}$s are similar in the same environment and dissimilar in different environments. However, since the environment label is unavailable in the unsupervised setting, we have to simultaneously learn Z and discover the cluster structures. To this end, we propose an intervention module to measure the similarities between each of pair of $\hat{z}_i$ and $\hat{z}_j$ as the probability of them belonging to the same environment. Furthermore, we then introduce a relational head to aggregate $\hat{Z}$s with high probability using relation loss. By simultaneously updating the dynamics prediction and the relation loss, we can cluster $\hat{Z}$s from the same environment, and learn an augmented dynamics prediction model $\hat{f}$. Next, we will give details about our relational intervention approach.

3.3 Relational Context Encoder

To learn the environment-specified factor Z of each environment, we firstly introduce a relational encoder g parameterized by ϕ. Similar to previous methods (Nagabandi et al., 2018a; Rakelly et al., 2019; Zhou et al., 2019; Lee et al., 2020; Seo et al., 2020), we use the past transition segments $\tau_{t-k:t-1} = \{(s_{t-k}, a_{t-k}), ..., (s_{t-1}, a_{t-1})\}$ as the input of g to estimate its corresponding $\hat{z}_{t-k:t-1}$:

$$\hat{z}_{t-k:t-1} = g(\tau^i_{t-k:t-1}; \phi).$$

After obtaining environment-specified $\hat{z}_{t-k:t-1}$ at timestep t, we incorporate it into the dynamics prediction model $\hat{f}$ to improve its generalization ability on different dynamics by optimizing the objective function following (Lee et al., 2020; Seo et al., 2020; Janner et al., 2019):

$$\mathcal{L}^{pred}_{\theta,\phi} = -\frac{1}{N}\sum_{i=1}^{N} \log\ \hat{f}(s^i_{t+1}|s^i_t, a^i_t, g(\tau^i_{t-k:t-1};\phi);\theta), \tag{1}$$

where k is the length of transition segments, t is the current timestep and N is the sample size. In practice, we sub-sample a mini-batch of data from the whole dataset to estimate (1) and use stochastic gradient descent to update the model parameters.

However, as analyzed in Section 3.2, the vanilla prediction error (1) is not sufficient to capture environment-specified Z of each environment, and even introduce redundant information into it. In order to eliminate the redundant information within transition segments and preserve the trajectory invariant information, we introduce a relational head (Patacchiola & Storkey, 2020) as a learnable function h to pull factors $\hat{Z}$ from the same trajectory together and push away those from different trajectories. Concretely, the estimated $\hat{z}^i_{t-k:t-1}$ in a mini-batch will be firstly aggregated as pairs, *e.g.* concatenate two factors as $[\hat{z}^i, \hat{z}^j]$, and the pairs having two factors from the same trajectory are seen as positives, and vice versa. Then the relational head h parameterized by φ takes a pair of aggregated factors as input to quantify the similarity of given two factors and returns a similarity score $\hat{y}$. To increase the similarity score $\hat{y}$ of positive pairs and decrease those negatives, we minimize the following objective:

$$\mathcal{L}^{relation}_{\varphi,\phi} = -\frac{1}{N(N-1)}\sum_{i=1}^{N}\sum_{j=1}^{N}\Big[\, y^{i,j}\cdot\log\ h([\hat{z}^i,\hat{z}^j];\varphi)+(1-y^{i,j})\cdot\log\,(1-h([\hat{z}^i,\hat{z}^j];\varphi))\Big], \tag{2}$$

where $y^{i,j}$ = 1 stands for positive pairs, and $y^{i,j}$ = 0 stands for negatives. Because the positive pairs have two factors belonging to the same trajectory, optimizing (2) can increase the similarity of $\hat{Z}$s estimated from the same trajectory, and push away those factors estimated from different trajectories in their semantical space. Therefore, by optimizing (2), the information that is invariant within a trajectory will be encoded into $\hat{Z}$ and the redundant information in transition segments will be reduced. (2) can also be interpreted from the perspective of mutual information, if we regard the $\hat{Z}$s from the same trajectory as the positive pairs, optimizing (2) can be seen as maximizing the mutual information between $\hat{Z}$s from the same trajectory (Please refer to (Tsai et al., 2020) and Appendix A.5), and thus preserve the invariant information with the same trajectory. However, estimating trajectory invariant information is insufficient because the estimated $\hat{Z}$s in the same environment will also be pushed away, which may undermine the cluster compactness for estimated $\hat{Z}$s.

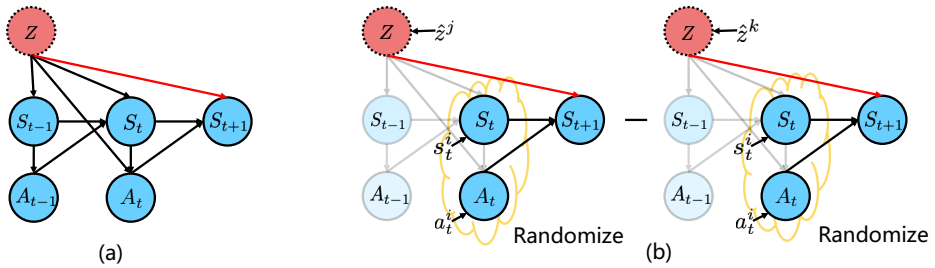

Figure 3: (a) The illustration of causal graph, and the red line denotes the direct causal effect from Z to S_{t+1}. (b) The illustration of estimating the controlled causal effect.

3.4 Interventional Prediction

Because the environment id of a trajectory is unknown, we cannot directly optimize relational loss (2) to cluster $\hat{Z}$ within an environment. We propose an interventional prediction method to find the trajectories belonging to the same environment. Here we formalize the dynamics prediction model using a graphical causal model, and the causal graph is illustrated as Figure 3 (a), where the next state S_{t+1} is caused by the current state S_t, action A_t and $\hat{Z}$, and the dynamics prediction model f represents the causal mechanism between them. Because Z from the same environment should have

the same influence on the states, and thus they should have the same causal effect on the next state S_{t+1} if given S_t and A_t under the causal framework. As such, we can find estimated $\hat{Z}$ belonging to the same environment by measuring the similarity of their causal effect on S_{t+1}. As Figure 3 (a) shows, there are multiple paths from Z to S_{t+1} and we roughly categorize them into two categories. The first category is the direct path between Z and S_{t+1} (shown as read in Figure 3). The second category contains all the indirect paths where Z influences S_{t+1} via previous states and actions. However, because the mediator in other paths *e.g.* S_t, A_t, may amplify or reduce the causal effect of Z, we only consider the direct path from Z to the next state(denote by the red line at Figure 3 (a)), which means that we need to block all paths with meditors from $\hat{Z}$ to S_{t+1}. By means of do-calculus (Pearl, 2000), we can estimate the direct causal effect of changing $Z = \hat{z}^j$ to $Z = \hat{z}^k$ on S_{t+1} through calculating the controlled direct effect (CDE) (Pearl, 2013) by intervening mediators and $\hat{Z}$:

$$CDE_{\hat{z}^j,\hat{z}^k}(s_t, a_t) = \mathbb{E}[S_{t+1}|do(S_t = s_t, A_t = a_t), do(Z = \hat{z}^j)] - \mathbb{E}[S_{t+1}|do(S_t = s_t, A_t = a_t), do(Z = \hat{z}^k)] \tag{3}$$

$$= \mathbb{E}[S_{t+1}|S_t = s_t, A_t = a_t, Z = \hat{z}^j] - \mathbb{E}[S_{t+1}|S_t = s_t, A_t = a_t, Z = \hat{z}^k], \tag{4}$$

where do is the do-calculus (Pearl, 2000). There is no arrow entering $\hat{Z}$, so the do operator on $\hat{Z}$ can be removed. Also, since there is no confounder between the mediators (S_t, A_t) and S_{t+1}, so we can remove the do operator of them as well, and the equation become as (4). Because the direct causal effects may differ for different values of S_t and A_t, we should sample S_t and A_t independently of Z, *i.e.* sampling S_t and A_t (Pearl et al., 2016) uniformly to get the average controlled direct causal effect from $\hat{Z}$ to S_{t+1}. However, if we use the uniformly generated S_t and A_t, the sampled distribution may differ from the training distribution, resulting in inaccurate the next state prediction. As such, we directly sample S_t and A_t from the observational data. For the convenience of optimization, we only use a mini-batch of S_t and A_t pairs (s_t^i, a_t^i), and concatenate them with $\hat{z}^j$ and $\hat{z}^k$ to calculate the average controlled direct effect under $\hat{f}$:

$$ACDE_{\hat{z}^j,\hat{z}^k} = \frac{1}{N}\sum_{i=1}^{N}|CDE_{\hat{z}^j,\hat{z}^k}(s_t^i, a_t^i)|, \tag{5}$$

where N is the batch size, j and k are the id of $\hat{Z}$ estimated from two transition segments. Specifically, because the factors $\hat{z}$ estimated from the same trajectory should be the same, and thus we minimize their controlled direct effect 5 as $\mathcal{L}^{dist}$ between them in the optimization process. Now we can use the calculated $ACDE_{\hat{z}^j,\hat{z}^k}$ as the semantic distance $d^{j,k}$ between estimated $\hat{z}^i$ and $\hat{z}^j$, and thus we can aggregate factors $\hat{Z}$ estimated from similar trajectories by the proposed relational head h. As such, we apply a transformation to convert distance metric $d^{j,k}$ to a similarity metric $w \in (0, 1]$, which is $w^{j,k} = exp(\frac{-d^{j,k}}{\beta})$, where β is a factor controlling the sensitivity of the distance metric. Specifically, because the scale and size of state varies in different tasks, *e.g.* 3 dims in Pendulum but 20 dims in Half-Cheetah, the optimal β may vary in different task. As such, we apply the L2 normalization in the distance metric d to convert it as a relative distance within a single task, thus making the optimal β stable in different tasks. Then we can directly aggregate similar trajectories by extending the loss function (2) as follows:

$$\begin{aligned}\mathcal{L}_{\varphi,\phi}^{i-relation} = &-\frac{1}{N(N-1)}\sum_{i=1}^{N}\sum_{j=1}^{N}\Big[\,[y^{i,j} + (1-y^{i,j})\cdot w^{i,j}]\cdot \log\ h([\hat{z}^i, \hat{z}^j];\varphi) \\ &+ (1-y^{i,j})\cdot(1-w^{i,j})\cdot\log\,(1-h([\hat{z}^i,\hat{z}^j];\varphi))\Big],\end{aligned} \tag{6}$$

where the first term indicates that the factors from the different trajectories can be aggregated with the similarity weight w and 1 those from the same trajectory, and the second term means that factors from different trajectories should be pushed with each other with weight $1 - w$. Similar to the analysis in section 3.3, optimizing the loss function (6) can increase the similarity between $\hat{Z}$ with weight w, and push away from them with the weight $1 - w$. Because $\hat{Z}$s estimated from the same environment have similar effects, these factors will be assigned with high similarities (estimated by the intervention operation of our paper). By simultaneously updating the prediction loss (1) and intervention relation loss 6, estimated $\hat{Z}$s within the same environment will be aggregated, and the learned dynamics function $\hat{f}$ can learn the modals of transition dynamics according to the $\hat{Z}$ in different clusters. The training procedure of our approach can refer to Algorithm process in Appendix A.2.

4 EXPERIMENTS

In this section, we conduct experiment to evaluate the performance of our approach by answering the following questions:

- Can our approach reduce the dynamics prediction errors in model-based RL? (Section 4.2.1)
- Can our approach promote the performance of model-based RL on environments with unseen dynamics? (Section 4.2.2)
- Can our approach learn the semantic meaningful dynamics change? (Figuer 1 and AppendixA.13)
- Is the similarity of w measured by the intervention module reasonable? (Appendix A.7)
- Can solely relational learning improve the performance of model-based RL? (Section 4.3)

4.1 ENVIROMENTAL SETUP

Implementation Details Our approach includes three learnable functions, including relational encoder, relational head and prediction head. All three functions are constructed with MLP and optimized by Adam (Kingma & Ba, 2014) with 1e-3 learning rate. During the training procedure, the trajectory segments are randomly sampled from the same trajectory to break the temporal correlations of the training data, which was also adopted by (Seo et al., 2020). Specifically, the length of the transition segments is 10, and the hyper-parameters are the same for all experiments, and details can be found in Appendix A.1.

Datasets Following the previous methods (Lee et al., 2020; Seo et al., 2020), we perform experiments on classic control algorithm (Pendulum) from OpenAI gym (Brockman et al., 2016) and simulated robotics control tasks (HalfCheetah, Cripple-HalfCheetah, Ant, Hopper, Slim-Humanoid) from Mujoco physics engine (Todorov et al., 2012).

Dynamics Settings To change the dynamics of each environment, we follow previous methods (Zhou et al., 2019; Packer et al., 2019; Lee et al., 2020; Seo et al., 2020) to change the environmental parameters (*e.g.* length and mass of Pendulum) and predefine them in the training and test environmental parameters lists. At the training time, we randomly sample the parameters from the training parameter list to train our relational context encoder and dynamics prediction model. Then we test our model on the environments with unseen dynamics sampled from the test parameter list. Specifically, the predefined parameters in the test parameter list are outside the training range. The details about training and test parameter lists for each task are the same with (Lee et al., 2020), and all details are given in Appendix A.1.

Planning Following (Lee et al., 2020; Seo et al., 2020), we use the model predictive model (MPC) (Maciejowski, 2002) to select actions based on learned dynamics prediction model, and assume that the reward function of environments is known. Also, the cross-entropy method (CEM) (De Boer et al., 2005) is used to optimize action sequences for finding the best performing action sequences.

Baselines We compare our approach with following state-of-the-art model-based RL methods on dynamics generalization. Also, to show the performance gap between our method and supervised dynamics generalization, we perform the method using true environment label to cluster Z.

- Probabilistic ensemble dynamics model (PETS) (Kurutach et al., 2018): PETS employs an probabilistic dynamics models to capture the uncertainty in modeling and planning.
- Meta learning based model-based RL (ReBAL and GrBAL) (Nagabandi et al., 2018b;a): These methods train a dynamics model by optimizing a meta-objective (Finn et al., 2017), and update the model parameters by updating a hidden with a recurrent model or by updating gradient updates at the test time.
- Context-aware dynamics model (CaDM) (Lee et al., 2020): This method design several auxiliary loss including backward and future states prediction to learn the context from transition segments.
- Trajectory-wise Multiple Choice Learning (TMCL) (Seo et al., 2020): This method is the state-of-the-art model-based RL method on dynamics generalization, which introduces the multi-choice learning to cluster environments. For the fair comparison, we also report the performance of TMCL without adaptation in Figure 7.

- True Label: The method uses our relational head to cluster $\hat{Z}$ with the true environment label (not the ground-truth of Z),. All hyperparameters are same with our method for the fair comparison.

4.2 Performance Comparisons with Baselines

4.2.1 Prediction Error Comparisons

We first evaluate whether the dynamics model trained by our methods can predict next-states more accurately or not. Figure 4 shows that the average dynamics prediction error of dynamics prediction models trained by three methods (CaDM (Lee et al., 2020), TMCL (Seo et al., 2020) and ours). We can see that the dynamics model trained by our relational intervention method has superior prediction performance over other state-of-the-art methods, achieving the lowest prediction errors on almost all six tasks. Specifically, the prediction errors of our model are lower than others by a large margin in Hopper and Pendulum, outperforming the state-of-the-art methods by approximately 10%.

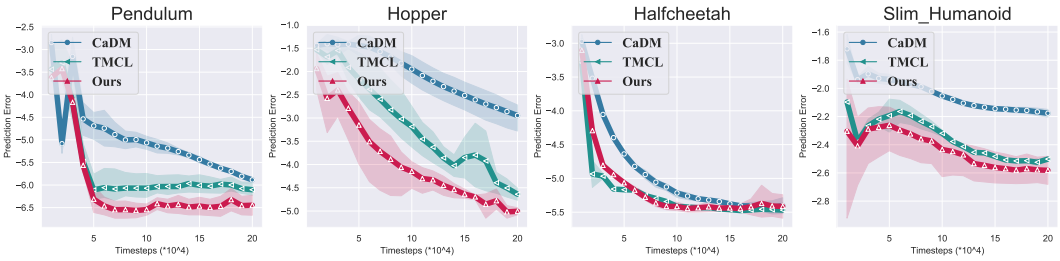

Figure 4: The average prediction errors of dynamics models on training environments during training process (over three times). Specifically, the x axis is the training timesteps and y axis is the log value of average prediction prediction errors. More figures are given at Appendix A.8.

Table 1: The average rewards of baseline model-based RL methods and ours on test environments with unseen dynamics. Here we report the average rewards over three runs (ours is ten). Specifically, the results of methods with $*$ are from the paper (Lee et al., 2020).

	PETS*	ReBAL*	GrBAL*	CaDM	TMCL	Ours	↑ Ratio
Pendulum	-1103	-943.6	-1137.9	-713.95±21.1	-691.2±93.4	**-587.5**±64.4	15.0%
Ant	965.883.5	63.0	44.7	1660±57.8	2994.9±243.8	**3297.9**±159.7	10.1%
Hopper	821.2	846.2	621	845.2±20.41	999.35±22.8	**1057.4**±37.2	5.8%
HalfCheetah	1720.9	52	-69.1	5876.6±799.0	9039.6±1065	**10859.2**±465.1	20.1%
C_HalfCheetah	1572	868.7	2814	3656.4±856.2	3998.8±856.2	**4819.3**±409.3	20.5%
Slim_Humanoid	784.5	97.25	-480.7	859.1±24.01	2098.7±109.1	**2432.6**±465.1	15.9%

4.2.2 Performance Comparisons

Then we evaluate the generalization of model-based RL agents trained by our methods and baselines on test environments with unseen dynamics. Following the setting of (Seo et al., 2020), we perform experiments three runs (ours with 10 runs to reduce random errors), and give the mean of rewards at Table 1. We can see that the meta-learning based methods (Nagabandi et al., 2018b;a) do not perform better than vanilla PETS (Kurutach et al., 2018), while methods (Lee et al., 2020; Seo et al., 2020) aiming to learn a generalized dynamics prediction model are superior to others significantly. Our approach achieves the highest rewards on all six tasks among all methods. Figure 5 shows that the mean and standard deviation of average rewards during the training procedure, indicating that the performance of our methods is better than the other two methods consistently at the training time, which is sufficient to show the superiority of our method over other methods. A fair comparison between TMCL (no adaptation) and our method can be found at Appendix A.6. Also, we observe that our method achieve comparable results with the method directly cluster $\hat{Z}$ using the truth environment label, which indicates that our intervention module actually can assign high similarities into $\hat{Z}$s estimated from the same environment in an unsupervised manner. The claim is also evaluated by the similarity visualization in the Appendix A.7, where we find that $\hat{Z}$s from the same environment will be assigned significant higher similarities than those pairs from different environments.

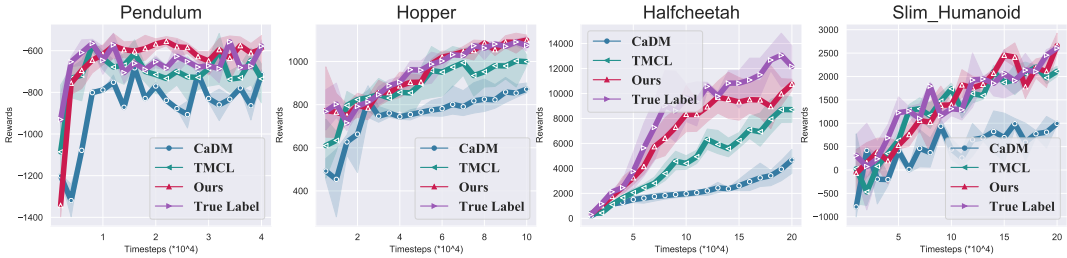

Figure 5: The average rewards of trained model-based RL agents on unseen environments. The results show the mean and standard deviation of returns averaged over three runs. The fair comparison between TMCL (no adaptation) and our method can be found in Appendix A.6

4.3 Ablation Study

In this section, we evaluate the effect of the proposed relation head and intervention prediction on the generalization improvement, respectively. Because the intervention prediction is based on the relational head, we compare the performance of our approach with and without the intervention. As Figure 6a and 6b show, after incorporating the relational head and intervention prediction, the performance of model-based agents and the generalization of the dynamics prediction model are both improved. However, although the model without the intervention module has lower prediction errors in the Pendulum task, it also has lower rewards than the whole model. One possible reason is that the Pendulum is simple for the dynamics prediction model to learn, and thus the dynamics prediction model with the vanilla relational head is a little over-fitting on the training environments (Please refer to prediction errors on test environments are given in Appendix A.9), limiting the performance improvement. This phenomenon confirms the importance of our intervention prediction on reducing the trajectory-specified redundant information.

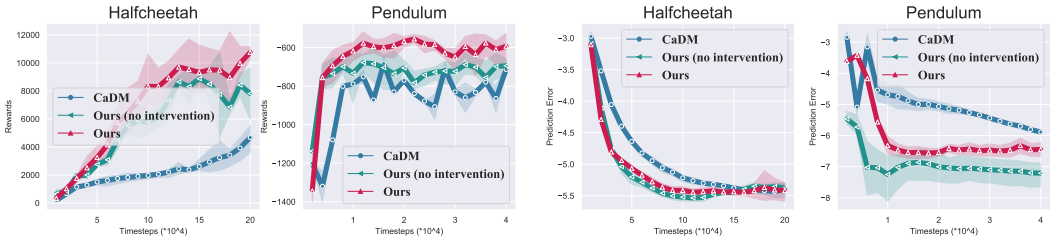

(a) (b)

Figure 6: (a) The average rewards of trained model-based RL agents on unseen environments. The results show the mean and standard deviation of returns averaged over three runs. (b) The average prediction errors over the training procedure. Prediction errors on test environments are given in Appendix A.9

5 Conclusion

In this paper, we propose a relational intervention approach to learn a generalized dynamics prediction model for dynamics generalization in model-based reinforcement learning. Our approach models the dynamics change as the variation of environment-specified factor $\mathcal{Z}$ and explicitly estimates $\mathcal{Z}$ from past transition segments. Because environment label is not available, it is challenging to extract $\mathcal{Z}$ from transition segments without introducing additional redundant information. We propose an intervention module to identify the probability of two estimated factors belonging to the same environment, and a relational head to cluster those estimated $\hat{Z}$s are from the same environments with high probability, thus reducing the redundant information unrelated to the environment. By incorporating the estimated $\hat{Z}$ into the dynamics prediction process, the dynamics prediction model has a stronger generalization ability against the change of dynamics. The experiments demonstrate that our approach can significantly reduce the dynamics prediction error and improve the performance of model-based agents on new environments with unseen dynamics.

6 ETHICS STATEMENT

Our paper provides a method to generalize the agent trained by the model-based reinforcement learning into new environments with unseen transition dynamics, which may significantly improve the robustness of trained agents in the complex real-world environment, thus broadening the application scenarios of robots trained by reinforcement learning. Although it is far away to apply such an algorithm to real-world applications, we still need to guard against the possible harm caused by its application in military robotics.

7 REPRODUCIBILITY STATEMENT

We have run our experiments over three runs (ours with 10 runs to reduce random errors) to reduce random errors, and public hyperparameters used in our experiments. We promise that we will public codes after the acceptance of this paper.

REFERENCES

Philip J Ball, Cong Lu, Jack Parker-Holder, and Stephen Roberts. Augmented world models facilitate zero-shot dynamics generalization from a single offline environment. *arXiv preprint arXiv:2104.05632*, 2021.

James Bannon, Brad Windsor, Wenbo Song, and Tao Li. Causality and batch reinforcement learning: Complementary approaches to planning in unknown domains. *arXiv preprint arXiv:2006.02579*, 2020.

Elias Bareinboim, Andrew Forney, and Judea Pearl. Bandits with unobserved confounders: A causal approach. *Advances in Neural Information Processing Systems*, 28:1342–1350, 2015.

Peter W Battaglia, Jessica B Hamrick, Victor Bapst, Alvaro Sanchez-Gonzalez, Vinicius Zambaldi, Mateusz Malinowski, Andrea Tacchetti, David Raposo, Adam Santoro, Ryan Faulkner, et al. Relational inductive biases, deep learning, and graph networks. *arXiv preprint arXiv:1806.01261*, 2018.

Konstantinos Bousmalis, Alex Irpan, Paul Wohlhart, Yunfei Bai, Matthew Kelcey, Mrinal Kalakrishnan, Laura Downs, Julian Ibarz, Peter Pastor, Kurt Konolige, et al. Using simulation and domain adaptation to improve efficiency of deep robotic grasping. In *2018 IEEE international conference on robotics and automation (ICRA)*, pp. 4243–4250. IEEE, 2018.

Greg Brockman, Vicki Cheung, Ludwig Pettersson, Jonas Schneider, John Schulman, Jie Tang, and Wojciech Zaremba. Openai gym. *arXiv preprint arXiv:1606.01540*, 2016.

Pieter-Tjerk De Boer, Dirk P Kroese, Shie Mannor, and Reuven Y Rubinstein. A tutorial on the cross-entropy method. *Annals of operations research*, 134(1):19–67, 2005.

Pim de Haan, Dinesh Jayaraman, and Sergey Levine. Causal confusion in imitation learning. *arXiv preprint arXiv:1905.11979*, 2019.

Finale Doshi-Velez and George Konidaris. Hidden parameter markov decision processes: A semiparametric regression approach for discovering latent task parametrizations. In *IJCAI: proceedings of the conference*, volume 2016, pp. 1432. NIH Public Access, 2016.

Chelsea Finn, Pieter Abbeel, and Sergey Levine. Model-agnostic meta-learning for fast adaptation of deep networks. In *International Conference on Machine Learning*, pp. 1126–1135. PMLR, 2017.

Andrew Forney, Judea Pearl, and Elias Bareinboim. Counterfactual data-fusion for online reinforcement learners. In *International Conference on Machine Learning*, pp. 1156–1164. PMLR, 2017.

Omer Gottesman, Fredrik Johansson, Joshua Meier, Jack Dent, Donghun Lee, Srivatsan Srinivasan, Linying Zhang, Yi Ding, David Wihl, Xuefeng Peng, et al. Evaluating reinforcement learning algorithms in observational health settings. *arXiv preprint arXiv:1805.12298*, 2018.

Shixiang Gu, Ethan Holly, Timothy Lillicrap, and Sergey Levine. Deep reinforcement learning for robotic manipulation with asynchronous off-policy updates. In *2017 IEEE international conference on robotics and automation (ICRA)*, pp. 3389–3396. IEEE, 2017.

Danijar Hafner, Timothy Lillicrap, Jimmy Ba, and Mohammad Norouzi. Dream to control: Learning behaviors by latent imagination. *arXiv preprint arXiv:1912.01603*, 2019a.

Danijar Hafner, Timothy Lillicrap, Ian Fischer, Ruben Villegas, David Ha, Honglak Lee, and James Davidson. Learning latent dynamics for planning from pixels. In *International Conference on Machine Learning*, pp. 2555–2565. PMLR, 2019b.

Han Hu, Jiayuan Gu, Zheng Zhang, Jifeng Dai, and Yichen Wei. Relation networks for object detection. In *Proceedings of the IEEE Conference on Computer Vision and Pattern Recognition*, pp. 3588–3597, 2018.

Michael Janner, Justin Fu, Marvin Zhang, and Sergey Levine. When to trust your model: Model-based policy optimization. *arXiv preprint arXiv:1906.08253*, 2019.

Lukasz Kaiser, Mohammad Babaeizadeh, Piotr Milos, Blazej Osinski, Roy H Campbell, Konrad Czechowski, Dumitru Erhan, Chelsea Finn, Piotr Kozakowski, Sergey Levine, et al. Model-based reinforcement learning for atari. *arXiv preprint arXiv:1903.00374*, 2019.

Nathan Kallus and Angela Zhou. Confounding-robust policy improvement. *arXiv preprint arXiv:1805.08593*, 2018.

Charles Kemp and Joshua B Tenenbaum. The discovery of structural form. *Proceedings of the National Academy of Sciences*, 105(31):10687–10692, 2008.

Diederik P Kingma and Jimmy Ba. Adam: A method for stochastic optimization. *arXiv preprint arXiv:1412.6980*, 2014.

B Ravi Kiran, Ibrahim Sobh, Victor Talpaert, Patrick Mannion, Ahmad A Al Sallab, Senthil Yogamani, and Patrick Pérez. Deep reinforcement learning for autonomous driving: A survey. *arXiv preprint arXiv:2002.00444*, 2020.

Daniel Kumor, Junzhe Zhang, and Elias Bareinboim. Sequential causal imitation learning with unobserved confounders. 2021.

Thanard Kurutach, Ignasi Clavera, Yan Duan, Aviv Tamar, and Pieter Abbeel. Model-ensemble trust-region policy optimization. *arXiv preprint arXiv:1802.10592*, 2018.

P. Langley. Crafting papers on machine learning. In Pat Langley (ed.), *Proceedings of the 17th International Conference on Machine Learning (ICML 2000)*, pp. 1207–1216, Stanford, CA, 2000. Morgan Kaufmann.

Finnian Lattimore, Tor Lattimore, and Mark D Reid. Causal bandits: Learning good interventions via causal inference. *arXiv preprint arXiv:1606.03203*, 2016.

Kimin Lee, Younggyo Seo, Seunghyun Lee, Honglak Lee, and Jinwoo Shin. Context-aware dynamics model for generalization in model-based reinforcement learning. In *International Conference on Machine Learning*, pp. 5757–5766. PMLR, 2020.

Sanghack Lee and Elias Bareinboim. Structural causal bandits: where to intervene? *Advances in Neural Information Processing Systems 31*, 31, 2018.

Ian Lenz, Ross A Knepper, and Ashutosh Saxena. Deepmpc: Learning deep latent features for model predictive control. In *Robotics: Science and Systems*. Rome, Italy, 2015.

Sergey Levine and Pieter Abbeel. Learning neural network policies with guided policy search under unknown dynamics. In *NIPS*, volume 27, pp. 1071–1079. Citeseer, 2014.

Chaochao Lu, Bernhard Schölkopf, and José Miguel Hernández-Lobato. Deconfounding reinforcement learning in observational settings. *arXiv preprint arXiv:1812.10576*, 2018.

Chaochao Lu, Biwei Huang, Ke Wang, José Miguel Hernández-Lobato, Kun Zhang, and Bernhard Schölkopf. Sample-efficient reinforcement learning via counterfactual-based data augmentation. *arXiv preprint arXiv:2012.09092*, 2020.

Clare Lyle, Amy Zhang, Minqi Jiang, Joelle Pineau, and Yarin Gal. Resolving causal confusion in reinforcement learning via robust exploration. In *Self-Supervision for Reinforcement Learning Workshop-ICLR 2021*, 2021.

Jan Marian Maciejowski. *Predictive control: with constraints*. Pearson education, 2002.

Volodymyr Mnih, Koray Kavukcuoglu, David Silver, Alex Graves, Ioannis Antonoglou, Daan Wierstra, and Martin Riedmiller. Playing atari with deep reinforcement learning. *arXiv preprint arXiv:1312.5602*, 2013.

Melissa Mozifian, Amy Zhang, Joelle Pineau, and David Meger. Intervention design for effective sim2real transfer. *arXiv preprint arXiv:2012.02055*, 2020.

Anusha Nagabandi, Ignasi Clavera, Simin Liu, Ronald S Fearing, Pieter Abbeel, Sergey Levine, and Chelsea Finn. Learning to adapt in dynamic, real-world environments through meta-reinforcement learning. *arXiv preprint arXiv:1803.11347*, 2018a.

Anusha Nagabandi, Chelsea Finn, and Sergey Levine. Deep online learning via meta-learning: Continual adaptation for model-based rl. *arXiv preprint arXiv:1812.07671*, 2018b.

Aaron van den Oord, Yazhe Li, and Oriol Vinyals. Representation learning with contrastive predictive coding. *arXiv preprint arXiv:1807.03748*, 2018.

Charles Packer, Katelyn Gao, Jernej Kos, Philipp Krähenbühl, Vladlen Koltun, and Dawn Song. Assessing generalization in deep reinforcement learning, 2019.

Massimiliano Patacchiola and Amos Storkey. Self-supervised relational reasoning for representation learning. *arXiv preprint arXiv:2006.05849*, 2020.

J Pearl. Causality: Models, reasoning, and inference 47cambridge university presscambridge, united kingdom. pearl, j. 2000. *Causality: models, reasoning, and inference*, 47, 2000.

Judea Pearl. Direct and indirect effects. *arXiv preprint arXiv:1301.2300*, 2013.

Judea Pearl, Madelyn Glymour, and Nicholas P Jewell. *Causal inference in statistics: A primer*. John Wiley & Sons, 2016.

Brenden K Petersen, Jiachen Yang, Will S Grathwohl, Chase Cockrell, Claudio Santiago, Gary An, and Daniel M Faissol. Precision medicine as a control problem: Using simulation and deep reinforcement learning to discover adaptive, personalized multi-cytokine therapy for sepsis. *arXiv preprint arXiv:1802.10440*, 2018.

Martin L Puterman. *Markov decision processes: discrete stochastic dynamic programming*. John Wiley & Sons, 2014.

Roberta Raileanu, Max Goldstein, Arthur Szlam, and Rob Fergus. Fast adaptation to new environments via policy-dynamics value functions. In *International Conference on Machine Learning*, pp. 7920–7931. PMLR, 2020.

Kate Rakelly, Aurick Zhou, Chelsea Finn, Sergey Levine, and Deirdre Quillen. Efficient off-policy meta-reinforcement learning via probabilistic context variables. In *International conference on machine learning*, pp. 5331–5340. PMLR, 2019.

David Raposo, Adam Santoro, David Barrett, Razvan Pascanu, Timothy Lillicrap, and Peter Battaglia. Discovering objects and their relations from entangled scene representations. *arXiv preprint arXiv:1702.05068*, 2017.

Steindór Sæmundsson, Katja Hofmann, and Marc Peter Deisenroth. Meta reinforcement learning with latent variable gaussian processes. *arXiv preprint arXiv:1803.07551*, 2018.

Adam Santoro, David Raposo, David GT Barrett, Mateusz Malinowski, Razvan Pascanu, Peter Battaglia, and Timothy Lillicrap. A simple neural network module for relational reasoning. *arXiv preprint arXiv:1706.01427*, 2017.

Adam Santoro, Ryan Faulkner, David Raposo, Jack Rae, Mike Chrzanowski, Theophane Weber, Daan Wierstra, Oriol Vinyals, Razvan Pascanu, and Timothy Lillicrap. Relational recurrent neural networks. *arXiv preprint arXiv:1806.01822*, 2018.

Julian Schrittwieser, Ioannis Antonoglou, Thomas Hubert, Karen Simonyan, Laurent Sifre, Simon Schmitt, Arthur Guez, Edward Lockhart, Demis Hassabis, Thore Graepel, et al. Mastering atari, go, chess and shogi by planning with a learned model. *Nature*, 588(7839):604–609, 2020.

Younggyo Seo, Kimin Lee, Ignasi Clavera, Thanard Kurutach, Jinwoo Shin, and Pieter Abbeel. Trajectory-wise multiple choice learning for dynamics generalization in reinforcement learning. *arXiv preprint arXiv:2010.13303*, 2020.

David Silver, Aja Huang, Chris J Maddison, Arthur Guez, Laurent Sifre, George Van Den Driessche, Julian Schrittwieser, Ioannis Antonoglou, Veda Panneershelvam, Marc Lanctot, et al. Mastering the game of go with deep neural networks and tree search. *nature*, 529(7587):484–489, 2016.

David Silver, Julian Schrittwieser, Karen Simonyan, Ioannis Antonoglou, Aja Huang, Arthur Guez, Thomas Hubert, Lucas Baker, Matthew Lai, Adrian Bolton, et al. Mastering the game of go without human knowledge. *nature*, 550(7676):354–359, 2017.

David Silver, Thomas Hubert, Julian Schrittwieser, Ioannis Antonoglou, Matthew Lai, Arthur Guez, Marc Lanctot, Laurent Sifre, Dharshan Kumaran, Thore Graepel, et al. A general reinforcement learning algorithm that masters chess, shogi, and go through self-play. *Science*, 362(6419): 1140–1144, 2018.

Flood Sung, Yongxin Yang, Li Zhang, Tao Xiang, Philip HS Torr, and Timothy M Hospedales. Learning to compare: Relation network for few-shot learning. In *Proceedings of the IEEE conference on computer vision and pattern recognition*, pp. 1199–1208, 2018.

Richard S Sutton and Andrew G Barto. *Reinforcement learning: An introduction*. MIT press, 2018.

Emanuel Todorov, Tom Erez, and Yuval Tassa. Mujoco: A physics engine for model-based control. In *2012 IEEE/RSJ International Conference on Intelligent Robots and Systems*, pp. 5026–5033. IEEE, 2012.

Yao-Hung Hubert Tsai, Han Zhao, Makoto Yamada, Louis-Philippe Morency, and Ruslan Salakhutdinov. Neural methods for point-wise dependency estimation. *arXiv preprint arXiv:2006.05553*, 2020.

Hado P van Hasselt, Matteo Hessel, and John Aslanides. When to use parametric models in reinforcement learning? *Advances in Neural Information Processing Systems*, 32:14322–14333, 2019.

Oriol Vinyals, Igor Babuschkin, Wojciech M Czarnecki, Michaël Mathieu, Andrew Dudzik, Junyoung Chung, David H Choi, Richard Powell, Timo Ewalds, Petko Georgiev, et al. Grandmaster level in starcraft ii using multi-agent reinforcement learning. *Nature*, 575(7782):350–354, 2019.

Sergei Volodin, Nevan Wichers, and Jeremy Nixon. Resolving spurious correlations in causal models of environments via interventions. *arXiv preprint arXiv:2002.05217*, 2020.

Lingxiao Wang, Zhuoran Yang, and Zhaoran Wang. Provably efficient causal reinforcement learning with confounded observational data. *arXiv preprint arXiv:2006.12311*, 2020.

Qi Wang and Herke van Hoof. Model-based meta reinforcement learning using graph structured surrogate models. *arXiv preprint arXiv:2102.08291*, 2021.

Russell A Wilke, Debbie W Lin, Dan M Roden, Paul B Watkins, David Flockhart, Issam Zineh, Kathleen M Giacomini, and Ronald M Krauss. Identifying genetic risk factors for serious adverse drug reactions: current progress and challenges. *Nature reviews Drug discovery*, 6(11):904–916, 2007.

Jiachen Yang, Brenden Petersen, Hongyuan Zha, and Daniel Faissol. Single episode policy transfer in reinforcement learning. *arXiv preprint arXiv:1910.07719*, 2019.

Yuxiang Yang, Ken Caluwaerts, Atil Iscen, Tingnan Zhang, Jie Tan, and Vikas Sindhwani. Data efficient reinforcement learning for legged robots. In *Conference on Robot Learning*, pp. 1–10. PMLR, 2020.

Vinicius Zambaldi, David Raposo, Adam Santoro, Victor Bapst, Yujia Li, Igor Babuschkin, Karl Tuyls, David Reichert, Timothy Lillicrap, Edward Lockhart, et al. Deep reinforcement learning with relational inductive biases. In *International Conference on Learning Representations*, 2018.

Amy Zhang, Zachary C Lipton, Luis Pineda, Kamyar Azizzadenesheli, Anima Anandkumar, Laurent Itti, Joelle Pineau, and Tommaso Furlanello. Learning causal state representations of partially observable environments. *arXiv preprint arXiv:1906.10437*, 2019a.

Amy Zhang, Clare Lyle, Shagun Sodhani, Angelos Filos, Marta Kwiatkowska, Joelle Pineau, Yarin Gal, and Doina Precup. Invariant causal prediction for block mdps. In *International Conference on Machine Learning*, pp. 11214–11224. PMLR, 2020a.

Amy Zhang, Shagun Sodhani, Khimya Khetarpal, and Joelle Pineau. Learning robust state abstractions for hidden-parameter block mdps. In *International Conference on Learning Representations*, 2020b.

Junzhe Zhang and Elias Bareinboim. Fairness in decision-making—the causal explanation formula. In *Thirty-Second AAAI Conference on Artificial Intelligence*, 2018.

Junzhe Zhang, Daniel Kumor, and Elias Bareinboim. Causal imitation learning with unobserved confounders. *Advances in neural information processing systems*, 33, 2020c.

Marvin Zhang, Sharad Vikram, Laura Smith, Pieter Abbeel, Matthew Johnson, and Sergey Levine. Solar: Deep structured representations for model-based reinforcement learning. In *International Conference on Machine Learning*, pp. 7444–7453. PMLR, 2019b.

Wenxuan Zhou, Lerrel Pinto, and Abhinav Gupta. Environment probing interaction policies. *arXiv preprint arXiv:1907.11740*, 2019.

A APPENDIX

We promise that we will public all codes after the acceptance of this paper.

A.1 ENVIRONMENTAL SETTINGS

We follow the environmental settings of Lee et al. (2020) in dynamics generalization. The details of settings are given as follows:

- **Pendulum** We modify the mass m and the length l of Pendulum to change its dynamics.
- **Half-Cheetah** We modify the mass of regid link m and the damping of joint d of Half-Cheetah agent to change its dynamics.
- **Crppled_Cheetah** We cripple the id of leg c of Half-Cheetah agent to change its dynamics.
- **Ant** We modify the mass of ant's leg m to change its dynamics. Specifically, we modify two legs by multiplying its original mass with m, and others two with $\frac{1}{m}$.
- **Slim_Humanoid** We modify the mass of rigid link m and the dampling of joint d of the Slim_Humanoid agent to change its dynamics.
- **Hopper** We modify the mass of m of the Hopper agent to change its dynamics.

The training and test modified parameter list can be found at the Table 2.

Table 2: The environmental settings in our paper.

	Training Parameter List	Test Parameter List	Episode Length
Pendulum	$m \in \{0.75,0.8,0.85,0.90,0.95,$ $1,1.05,1.1,1.15,1.2,1.25\}$ $l \in \{0.75,0.8,0.85,0.90,0.95,$ $1,1.05,1.1,1.15,1.2,1.25\}$	$m \in \{0.2,0.4,0.5,0.7,$ $1.3,1.5,1.6,1.8\}$ $l \in \{0.2,0.4,0.5,0.7,$ $1.3,1.5,1.6,1.8\}$	200
Half-Cheetah	$m \in \{0.75,0.85,1.00,1.15,1.25\}$ $d \in \{0.75,0.85, 1.00,1.15,1.25\}$	$m \in \{0.2,0.3,0.4,0.5,$ $1.5,1.6,1.7,1.8\}$ $d \in \{0.2,0.3,0.4,0.5,$ $1.5,1.6,1.7,1.8\}$	1000
C_Cheetah	$c \in \{0,1,2,3\}$	$c \in \{4,5\}$	1000
Ant	$m \in \{0.85,0.90,0.951.00\}$	$m \in \{0.20,0.25,0.30,0.35,0.40,$ $0.45,0.50,0.55,0.60\}$	1000
Slim_Humanoid	$m \in \{0.80,0.90,1.00,1.15,1.25\}$ $d \in \{0.80,0.90,1.00,1.15,1.25\}$	$m \in \{0.40,0.50,0.60,0.70,$ $1.50,1.60,1.70,1.80\}$ $d \in \{0.40,0.50,0.60,0.70,$ $1.50,1.60,1.70,1.80\}$	1000
Hopper	$m \in \{0.5, 0.75, 1.0, 1.25, 1.5\}$	$m \in \{0.25, 0.375, 1.75, 2.0\}$	500

A.2 ALGORITHM

The training procedure is give at Algorithm 1.

A.3 TRAINING DETAILS

Similar to the Lee et al. (2020), we train our model-based RL agents and relational context encoder for 20 epochs, and we collect 10 trajectories by a MPC controller with 30 horizon from environments at each epoch. In addition, the cross entropy method (CEM) with 200 candidate actions is chosen as the planing method. Specifically, the batch size for each experiment is 64, β is 5e-3. All module are learned by a Adam optimizer with 0.001 learning rate.

Algorithm 1 The training algorithm process of our relational intervention approach

Initialize parameters of relational encoder ϕ, dynamics prediction model θ and relational head φ
Initialize dataset $\mathcal{B} \leftarrow \emptyset$
for Each Iteration **do**
  sample environments $\mathcal{M}^i$ from training environments $\{\mathcal{M}_i^{tr}\}_{i=0}^K$ ▷ Collecting Data
  for $T = 1$ to TaskHorizon **do**
    Get the estimation of the environment-specified factor $\hat{z}^i_{t-k:t-1} = g(\tau^i_{t-k:t-1}; \phi)$
    Collect $(s_t, a_t, s_{t+1}, r_t, \tau^i_{t-k:t-1})$ from $\mathcal{M}^i$ with dynamics prediction model θ
    Update $\mathcal{B} \leftarrow \mathcal{B} \cup (s_t, a_t, s_{t+1}, r_t, \tau^i_{t-k:t-1})$
  end for
  for Each Dynamics Training Iteration **do** ▷ Update ϕ,θ and φ
    for $k = 1$ to K **do**
      Sample data $\tau^{i,b,P}_{t-k:t-1}$, $\tau^{i,b,K}_{t:M}$ and $\tau^{j,b,P}_{t-k:t-1}$, $\tau^{j,b,K}_{t:M}$ with batch size B,from $\mathcal{B}$
      Get the estimation of the environment-specified factor $\hat{z}^{i,B,,P}_{t-k:t-1} = g(\tau^{i,B,P}_{t-k:t-1}; \phi)$ and $\hat{z}^{ij,B,,P}_{t-k:t-1} = g(\tau^{j,B,P}_{t-k:t-1}; \phi)$
      Estimate the probability w of $\hat{z}^{i,B,,P}_{t-k:t-1}$ and $\hat{z}^{j,B,,P}_{t-k:t-1}$ belonging to the same environment.
      Compute the total loss
      $\mathcal{L}^{tot}$=$\mathcal{L}^{pred}_{\phi,\theta}(\tau^{i,B,,K}_{t:M}, \hat{z}^{i,B,,P}_{t-k:t-1}) + \mathcal{L}^{i-relation}_{\phi,\varphi}(\hat{z}^{i,B,,P}_{t-k:t-1}) + \mathcal{L}^{dist}_{\phi,\theta}(\tau^{i,B,K}_{t:M}, \hat{z}^{i,B,P}_{t-k:t-1})$
      Update θ , ϕ , $\varphi \leftarrow \nabla_{\theta,\phi\,\varphi} \frac{1}{B} \mathcal{L}^{tot}$
    end for
  end for
end for

A.4 Network Details

Similar to the Lee et al. (2020), the relational encoder is constructed by a simple 3 hidden-layer MLP, and the output dim of environmental-specific vector $\hat{z}$ is 10. The relational head is modelled as a single layer MLP with 10 units (same with the dim of $\hat{z}$) and an output layer. The dynamics prediction model is a 4 hidden-layer MLP with 200 units.

A.5 Connection between Relation Loss and Mutual Information

Given a pair of data $(x, y) \in \mathcal{X} \times \mathcal{Y}$, we donote the joint distribution of X and Y are P_{XY}, and their marginal distributions are P_X and P_Y, respectively. By definition, the mutual information between X and Y is:

$$I(X;Y) = \mathbb{E}_{P_{XY}}[\log(\frac{p(x,y)}{p(x)p(y)})] \tag{7}$$

To estimate mutual information between X and Y, (Tsai et al., 2020) proposes a probabilistic classifier method. Concretely, we can use a Bernoulli random variable C to classify one given data pair (x, y) from the joint distribution P_{XY} $(C = 1)$ or from the product of marginal distribution $P(X)P(Y)$ $(C = 0)$. Therefore, the mutual information $I(X;Y)$ between X and Y can be rewrite as:

$$\begin{aligned} I(X;Y) &= \mathbb{E}_{P_{XY}}[\log(\frac{p(x,y)}{p(x)p(y)})] \\ &= \mathbb{E}_{P_{XY}}[\log(\frac{p(x,y|C=1)}{p(x,y|C=0)})] \\ &= \mathbb{E}_{P_{XY}}[\log(\frac{p(C=0)P(C=1|x,y)}{p(C=1)P(C=0|x,y)})] \end{aligned} \tag{8}$$

Obviously, $\frac{p(C=0)}{p(C=1)}$ can be approximated by the sample size, *i.e.* $\frac{n_{P_X P_Y}}{n_{P_{XY}}}$, while $\frac{P(C=1|x,y)}{P(C=0|x,y)}$ can be measured by a classifier $h(C|x, y)$, and it can be learned by our relation loss with relational head h:

$$\mathcal{L}^{relation}_{\varphi,\phi} \;=\; -\Big[\, C \cdot \log\; h([x,y];\varphi) + (1-C) \cdot \log\,(1 - h([x,y];\varphi))\Big], \tag{9}$$

where $C = 1$ if the given pair (x, y) is from the joint distribution P_{XY}, and $C = 0$ if the given pair (x, y) is from the product of the marginal distributions $P_X P_Y$. Because $\frac{p(C=0)}{p(C=1)}$ tend to be a constant, optimizing our relation loss is actually estimating the mutual information $I(X;Y)$ between X and Y. As such, if we regard the pairs of $(\hat{z})$ from the same trajectory/environment as positive pairs, and others are negative pairs, optimizing 2 is actually maxmizing the mutual information between between $(\hat{z})$ from the same trajectory/environment, and thus preserve the trajectory/environment invariant information. If the readers are interested at the concrete bound about this method to estimate mutual information, please refer to (Tsai et al., 2020).

A.6 Fair Comparison with TMCL

Because TMCL need an adaptation process when deploying it into the real-world while our method does not. For the fair comparison and show the significance of our method over TMCL, we test the performance of TMCL with no adaptation, and show the results below:

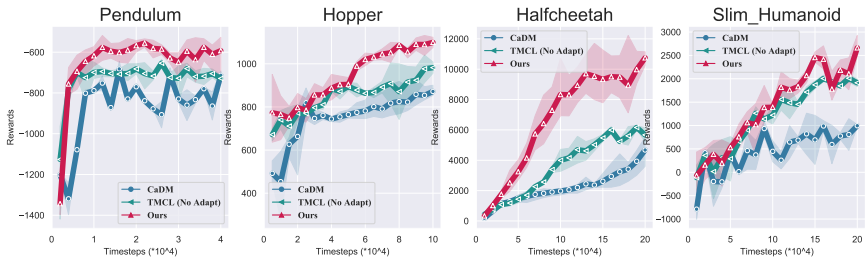

Figure 7: The estimated similarities between $\hat{Z}$s (learned by the model without Intervention module) from different environments and anchors (mass=1) on different tasks, where the box represent the range of 50% samples, the line in the middle of a box denotes the average similarity and the top/bottom lines denote the max/min similarities.

We can see that the average returns of TMCL without adaptation are significantly lower than ours, especially for classic control task Halfcheetah, which is a direct evidence to support our claim: environment-separated Zs is important for the generalization of dynamics functions, and our method can significantly outperform baselines in zero-shot unseen test environments with different dynamics. Specifically, the performance of TMCL with no adaptation is still superior to the CaDM, this is because TMCL use the invariance of Z within an trajectory (Z should predict other states within a trajectory in TMCL), which is similar to our paper with no intervention module.

A.7 Similarities Visualiaztion

To evaluate the correctness of the estimated similarity of our intervention module, we use a $\hat{z}^i$ estimated from the environment where the mass is 1 as the anchor, and randomly sample 200 $\hat{z}^j$ estimated from different environments (including mass = 1). Then we calculate the similarity between anchor $\hat{z}^i$ and $\hat{z}^j$, and visualize the similarities according to their environments. As Figure 8 shows, $\hat{z}^j$s belonging to the same environment with the anchor $\hat{z}^i$ have significant higher similarities than those belonging to other environments, and even higher than 0.8 in some tasks (all are higher than 0.6), which shows that our intervention module can successfully identify whether two $\hat{z}$s from the same environment or not.

To study the role of intervention module, we also visualize the similarity of $\hat{z}^i$ learned by the model without intervention module, and the results are given as Figure 9. Figure 9 shows that many contexts from different environments still have high similarities. This indicates that the existing relational learning cannot separate environment-specified factors Zs. By contrast, after incorporating the intervention module, the contexts from different environments have significantly smaller similarities than those from the same environments. The comparison between Figures 8 and 9 directly shows that our intervention module is valuable to predict whether two contexts are from the same environment or not.

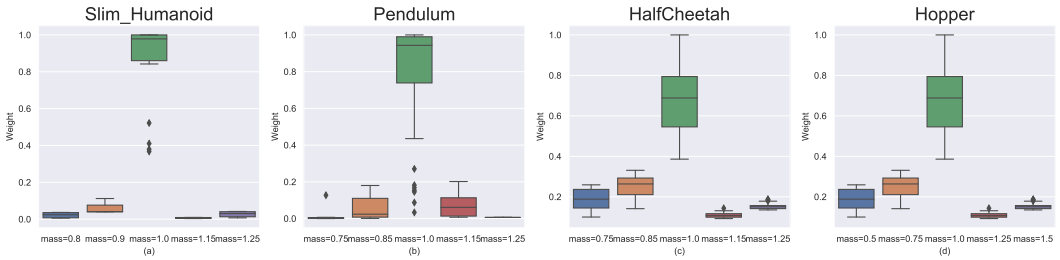

Figure 8: The estimated similarities between $\hat{Z}$s (learned by the model with Intervention module) from different environments and anchors (mass=1) on different tasks, where the box represent the range of 50% samples, the line in the middle of a box denotes the average similarity and the top/bottom lines denote the max/min similarities.

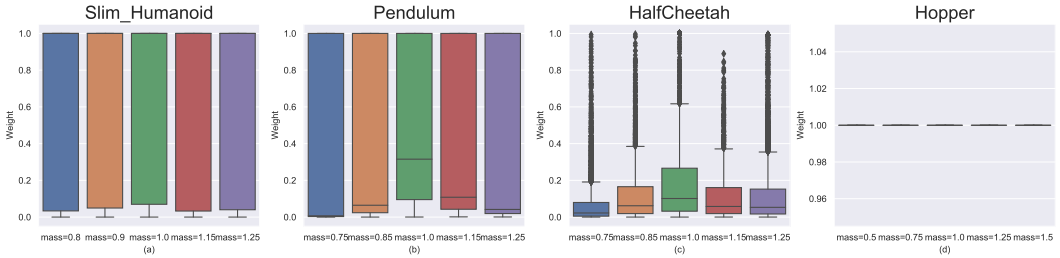

Figure 9: The estimated similarities between $\hat{Z}$s (learned by the model without Intervention module) from different environments and anchors (mass=1) on different tasks, where the box represent the range of 50% samples, the line in the middle of a box denotes the average similarity and the top/bottom lines denote the max/min similarities.

A.8 Prediction Errors on Traing Environments

The prediction errors of each method on training environment are given at Figure 10.

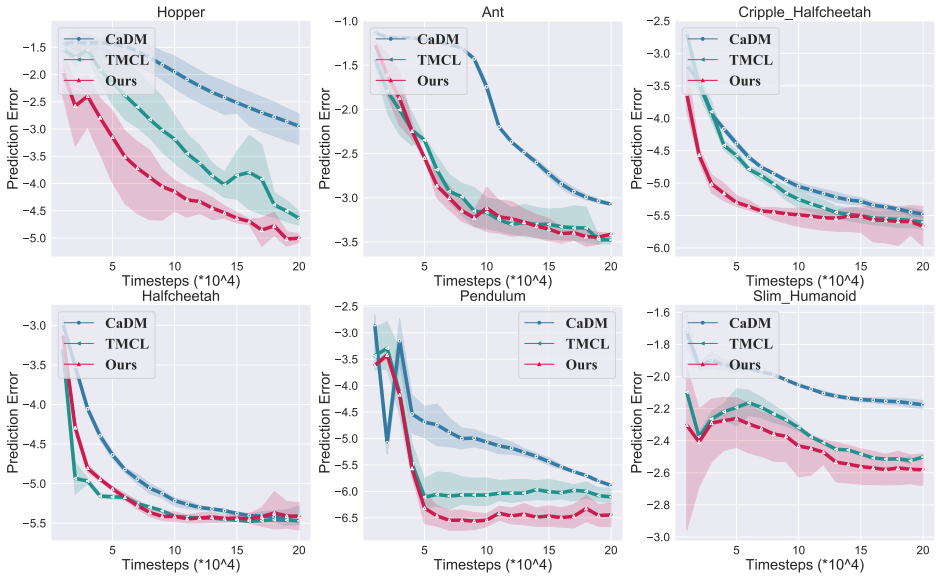

Figure 10: The average prediction errors of dynamics models on training environments during training process (over three times). Specifically, the x axis is the training timesteps and y axis is the log value of average prediction prediction errors. More figures are given at Appendix A.8.

A.9 PREDICTION ERRORS ON TEST ENVIRONMENTS

The prediction errors of each method on test environments are given at Table 3. Specifically, we test each test environment 10 times, and plot the average prediction error to reduce random errors (Figure 11).

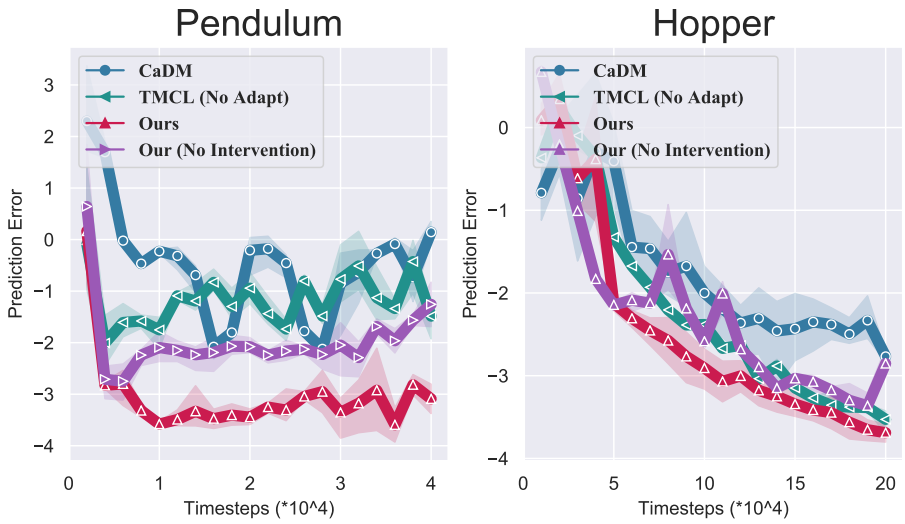

Figure 11: The average prediction errors of dynamics models on test environments during training process (over three times). Specifically, the x axis is the training timesteps and y axis is the average *log* value of prediction prediction errors.

Table 3: The prediction errors of methods on test environments

	CaDM (Lee et al., 2020)	TMCL (Seo et al., 2020)	Ours
Hopper	0.0551± 0.0236	0.0316 ± 0.0138	**0.0271 ± 0.0011**
Ant	0.3850 ± 0.0256	0.1560 ± 0.0106	**0.1381 ± 0.0047**
C_Halfcheetah	0.0815 ± 0.0029	0.0751 ±0.0123	**0.0525 ± 0.0061**
HalfCheetah	0.6151 ± 0.0251	1.0136 ± 0.6241	**0.4513 ±0.2147**
Pendulum	0.0160 ±0.0036	0.0130± 0.0835	**0.0030 ± 0.0012**
Slim_Humanoid	0.8842 ± 0.2388	0.3243 ± 0.0027	**0.3032 ± 0.0046**

A.10 PREDICTION ERRORS ON SPECIFIED ENVIRONMENT

The prediction errors of each method on specified environment are given at Table 4, 5 and 6.

Table 4: The prediction errors of methods on specified environment of Hopper Task.

mass	CaDM (Lee et al., 2020)	TMCL (Seo et al., 2020)	Ours
0.25	0.0443 ± 0.0049	0.0294 ± 0.0131	**0.0120 ± 0.0025**
1.75	0.0459 ± 0.0006	0.0131 ± 0.0138	**0.0132 ± 0.0013**

Table 5: The prediction errors of methods on specified environment of Ant Task.

mass	CaDM (Lee et al., 2020)	TMCL (Seo et al., 2020)	Ours
0.30	0.0928 ± 0.0019	0.0910 ± 0.0200	**0.0669 ± 0.0040**
0.50	0.1013 ± 0.0057	0.0887 ± 0.0212	**0.0671 ± 0.0034**

A.11 THE AVERAGE RETURNS ON TEST ENVIRONMENTS DURING TRAINING PROCESS

The average returns on test environments during training process are given at Figure 12.

Table 6: The prediction errors of methods on specified environment of Slim_Humanoid Task.

mass	CaDM (Lee et al., 2020)	TMCL (Seo et al., 2020)	Ours
0.50	0.1614 ± 0.0165	0.1860 ± 0.0040	$\mathbf{0.1282 \pm 0.0295}$
0.70	0.1512 ± 0.0152	0.1550 ± 0.0186	$\mathbf{0.1236 \pm 0.0162}$
1.50	0.1601 ± 0.0202	0.1873 ± 0.0087	$\mathbf{0.1444 \pm 0.0233}$
1.70	0.1439 ± 0.02029	0.1688 ± 0.01032	$\mathbf{0.1217 \pm 0.0206}$

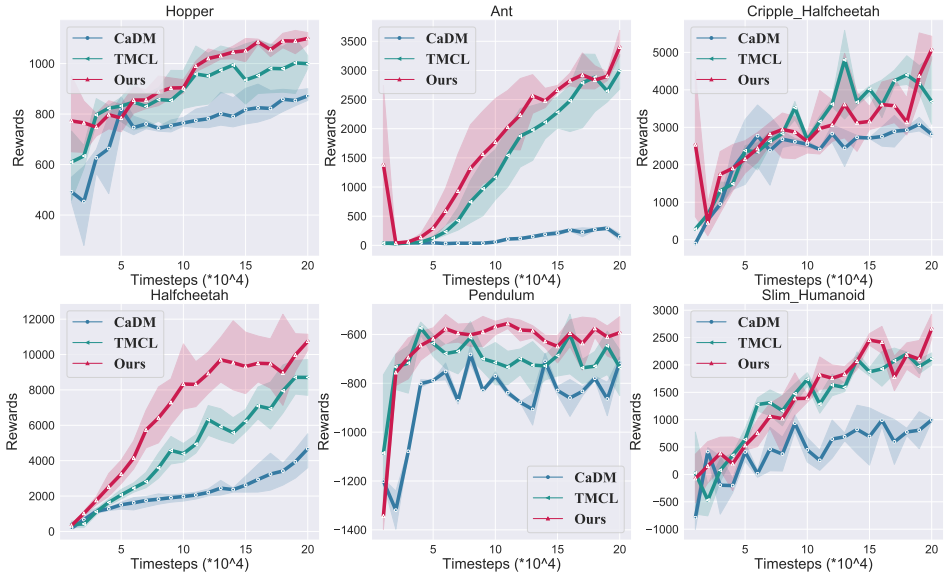

Figure 12: The average rewards of trained model-based RL agents on unseen environments. The results show the mean and standard deviation of returns averaged over three runs.

A.12 Quantitative Clustering Performance Comparison

To quantitatively evaluate the $\hat{Z}$s' clustering performance, we use K-means algorithm to predict each Z's environment id, and compare them with the true environment id. The details are provided in demo of K-means and evaluation metrics. The results are given at below. Specifically, TMCL has lower clustering performances than CaDM, but TMCL still has higher returns on test environments than CaDM. This is because TMCL clusters environments via multiplying dynamics functions rather than separating Zs.

Table 7: Quantitatively clustering evaluation results of $\hat{Z}$ on Pendulum.

	homo	compl	v-meas	ARI	AMI
CaDM	1	0.655	0.627	0.516	0.599
TMCL	0	0.298	0.217	0.088	0.165
Ours (no Intervention)	0	0.768	0.762	0.760	0.653
Ours	**1**	**0.932**	**0.932**	**0.937**	**0.931**

Table 8: Quantitatively clustering evaluation results of $\hat{Z}$ on Halfcheetah.

	homo	compl	v-meas	ARI	AMI
CaDM	0	0.262	0.260	0.203	0.257
TMCL	0	0.239	0.165	0.051	0.126
Ours (no Intervention)	0	0.368	0.362	0.265	0.353
Ours	0	**0.416**	**0.411**	**0.312**	**0.405**

Table 9: Quantitative clustering evaluation results of $\hat{Z}$ on Slim_Humanoid.

	homo	compl	v-meas	ARI	AMI
CaDM	0	0.046	0.045	0.027	0.042
TMCL	0	0.002	0.002	0.000	0.000
Ours	0	**0.055**	**0.052**	**0.037**	**0.058**

Table 10: Quantitative clustering evaluation results of $\hat{Z}$ on Cripple_Halfcheetah.

	homo	compl	v-meas	ARI	AMI
CaDM	1	0.733	0.716	0.686	0.701
TMCL	0	0.253	0.000	0.000	0.000
Ours	**1**	**0.853**	**0.851**	**0.860**	**0.849**

Table 11: Quantitative clustering evaluation results of $\hat{Z}$ on Hopper.

	homo	compl	v-meas	ARI	AMI
CaDM	0	0.019	0.018	0.010	0.015
TMCL	0	0.023	0.008	0.000	0.003
Ours	0	**0.130**	**0.108**	**0.049**	**0.089**

According to the quantitative clustering performance measures, we can see that the clustering performance of our method is superior to baselines by a large margin, and the results are consistent with the performance on the test environments.

A.13 VISUALIZATION

A.14 T-SNE VISUALIZATION

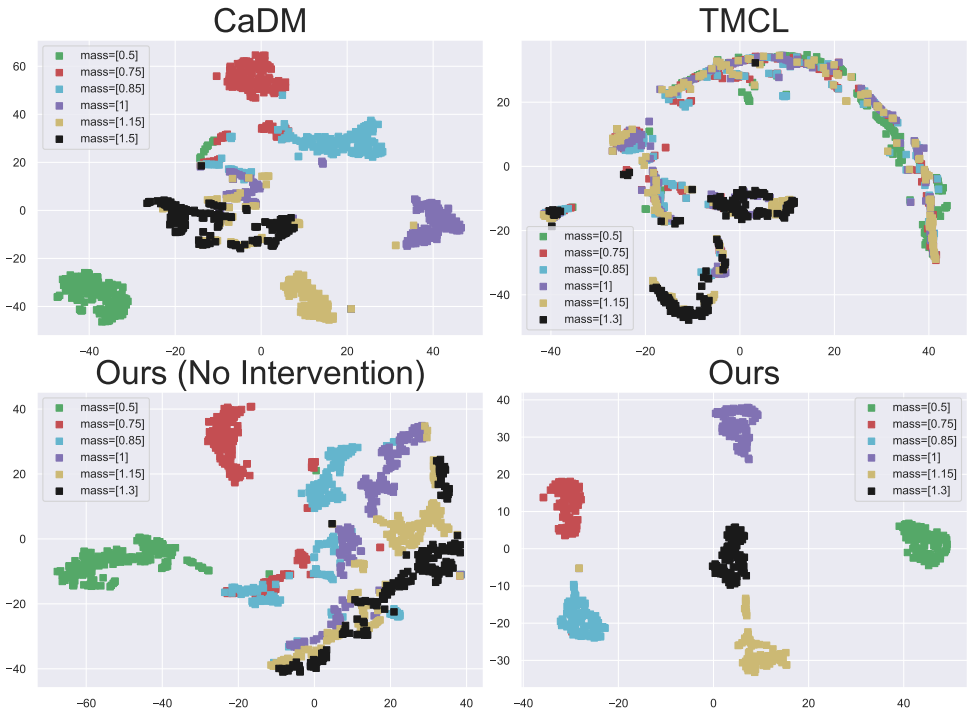

Figure 13: The T-SNE visualization of estimated context (environmental-specific) vectors in the **Pendulum** task, where mass = 0.5 and mass =1.3 are from test environments.

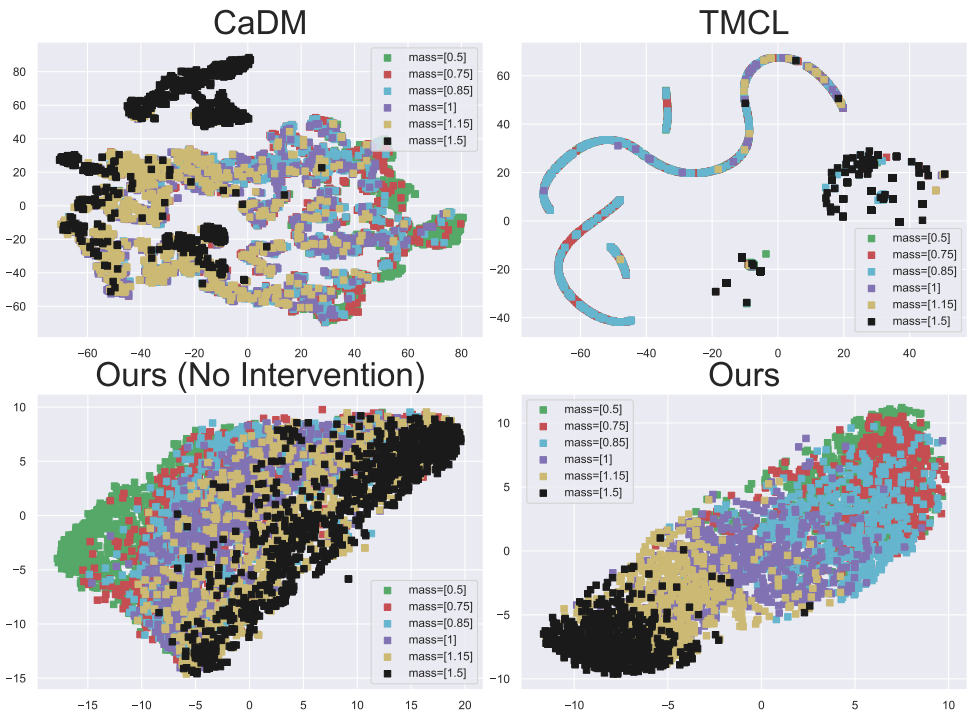

Figure 14: The T-SNE visualization of estimated context (environmental-specific) vectors in the **Halfcheetah** task, where mass = 0.5 and mass =1.5 are from test environments.

A.15 PCA Visualization

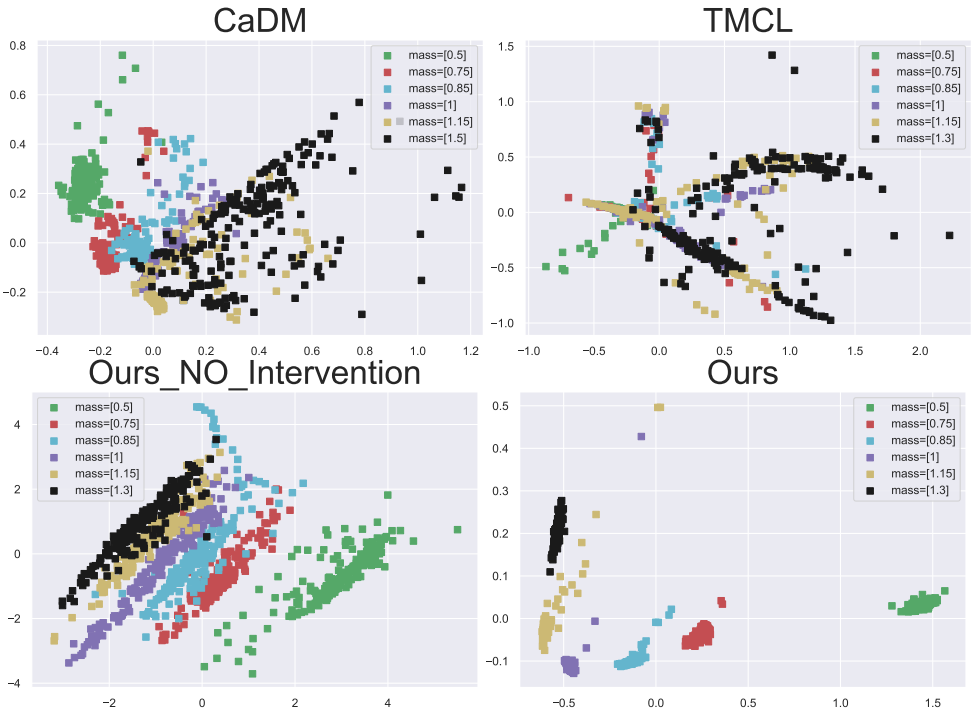

Figure 15: The PCA of estimated context (environmental-specific) vectors in **Pendulum** task, where mass = 0.5 and mass =1.3 are from test environments.

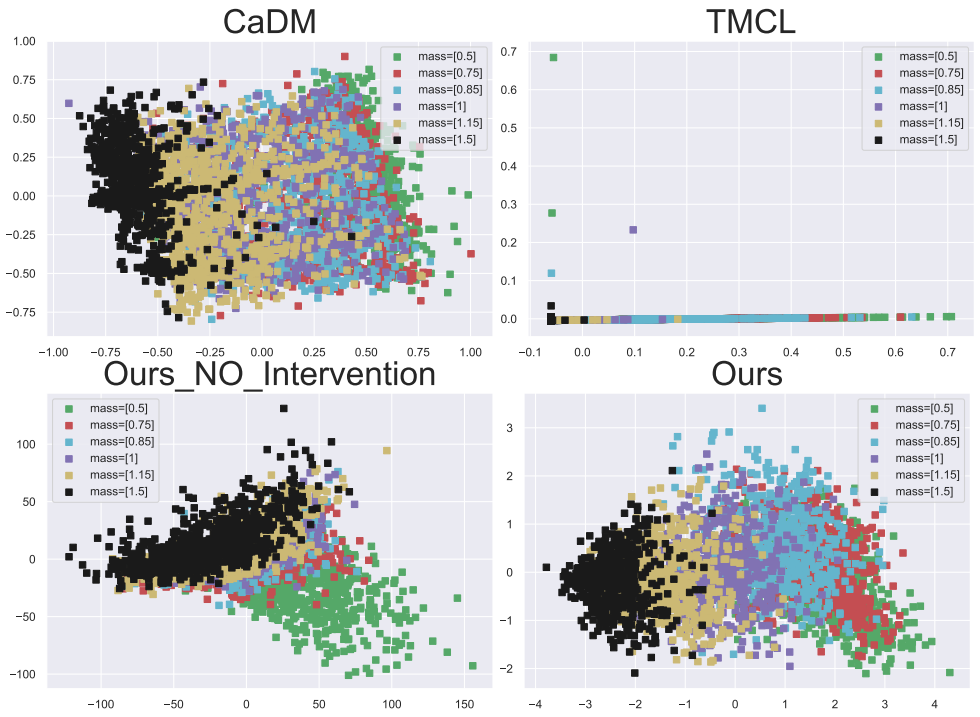

Figure 16: The PCA of estimated context (environmental-specific) vectors in **HalfCheetah** task, where mass = 0.5 and mass =1.5 are from test environments.

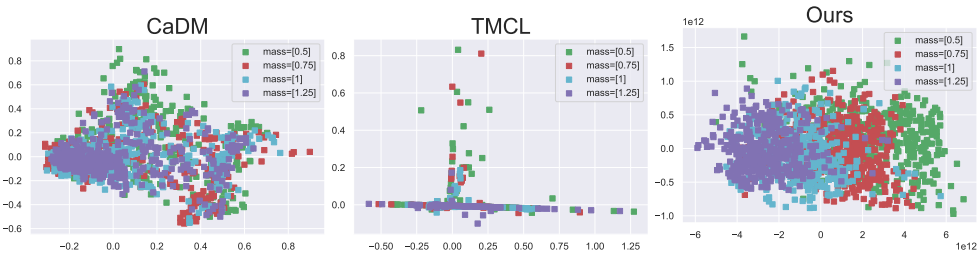

Figure 17: The PCA of estimated context (environmental-specific) vectors in the **Hopper** task.

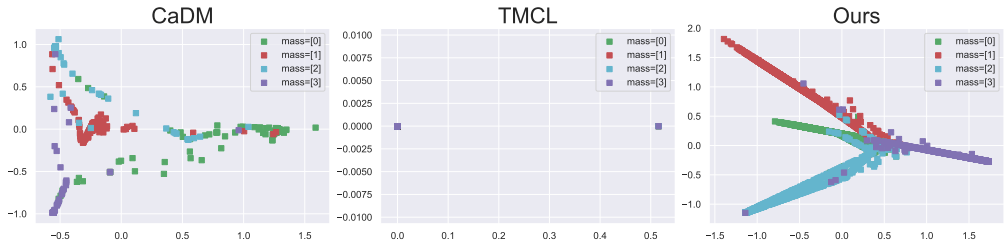

Figure 18: The PCA of estimated context (environmental-specific) vectors in the **Cripple_Halfcheetah** task.

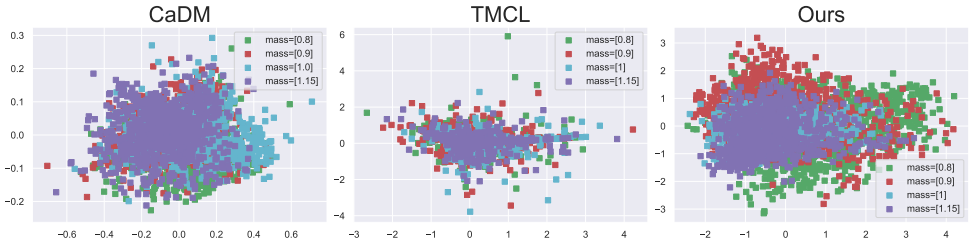

Figure 19: The PCA of estimated context (environmental-specific) vectors in the **Slim_Humanoid** task.